

Molecular Stiffness of Individual Hyperbranched Macromolecules at Solid Surfaces

Hennady Shulha, Xiaowen Zhai, and Vladimir V. Tsukruk*

Department of Materials Science & Engineering, Iowa State University, Ames, Iowa 50011

Received September 5, 2002

ABSTRACT: The elastic properties of dendritic (hyperbranched) molecules with dimensions below 3 nm have been probed with atomic force microscopy (AFM), which allows for the micromapping of the surface stiffness with nanoscale resolution. To anchor dendritic molecules with hydroxyl terminal groups and reduce tip–molecule interactions, a modification of the silicon surface with an amine-terminated self-assembled monolayer (SAM) and AFM tips with methyl-terminated SAMs was used. The nanomechanical response was analyzed in the terms of sequential deformation of dendritic molecules and alkyl-silane monolayers. We observed higher elastic modulus of individual dendritic molecules of the fourth generation in comparison with the corresponding third generation (350 vs 190 MPa). This difference is caused by more shape persistent properties of dendritic molecules with denser shells. Higher stiffness was also revealed for molecules within long-chain aggregates as compared to individual molecules and small aggregates. We speculate that this is caused by additional lateral constraints due to the presence of densely packed neighboring “border” molecules tethered to the supporting substrate.

Introduction

An understanding of nanomechanical properties of individual organic and polymeric molecules and their molecular aggregates is critical for the design of the nanoscale contact interactions in nanodevices of electromechanical and fluidic types.^{1,2} Current approaches are limited by qualitative visualization of the surface distribution with atomic force microscopy (AFM). A lateral resolution usually is appropriate for the observation of individual molecules or their aggregates even considering significant tip dilation.³ Alternatively, within a force spectroscopy approach, force–distance curves are collected for multiple, unspecified surface locations, and pull-off forces are used for the evaluation of specific interactions or the tensile properties of molecules.^{4–6} Direct correlation between the surface nanostructure and the nanomechanical properties could not be readily obtained within this approach. A main disadvantage of this method is that an object studied, as a rule, should be long (usually hundreds of nanometers). Many experiments, thus, are focused on DNA, proteins, and high molecular weight functionalized macromolecules. Another problem of this method is that, without concurrent topographical measurements, it is difficult to determine what was, in fact, being stretched: molecules, bundles of molecules, substrate, or something else.^{7–9}

An alternative approach includes the micromapping of selected surface areas via a collection of so-called force–volume (FV) data composed of an array of force–distance curves and the analysis of the indentation–deflection behavior with the AFM tip engaged in compression mode.¹⁰ Under optimal probing conditions, an application of the contact mechanics model to this compression mode (either Hertzian or Sneddon) could produce a reliable value of the elastic modulus, surface distribution of surface stiffness or elasticity, and even the depth profile of the elastic modulus.¹¹ This approach

is applicable to molecularly thick compliant films, nanoscale colloidal particles, and nanoparticulate molecules and can provide reliable information with lateral resolution below 10 nm and vertical resolution below 0.2 nm.^{10,11}

In this paper, we report on measurements of the elastic properties (stiffness or elastic modulus) of individual nanoparticulate molecules with an effective diameter below 3 nm and their surface aggregates containing a limited number of molecules (several dozens). We selected dendritic molecules, namely hyperbranched polyesters, which are known for forming compliant nanoparticulates with a diameter of several nanometers. Internal architecture of these molecules could be represented as a highly branched, treelike structure with a central core, branches, a certain level of internal cyclization, and a high concentration of terminal functional groups (Figure 1).^{12–14} These molecules represent a new class of functionalized materials with promising interfacial nanoscale properties as discussed in recent publications.^{15–17} Unlike regular dendrimers, their chemical microstructure contains significant fraction of defects, a degree of branching does not exceed usually 60–70%, and they possess modest polydispersity.¹⁸ However, they still demonstrate characteristic properties of unique nanoparticulate molecules and might serve as substitutes for expensive dendrimers materials for less demanding applications.

To collect reliable nanomechanical data, the micromapping of the surface stiffness with a nanoscale resolution should be carefully designed. To enhance the surface stability of the molecular aggregates and provide ideal landscape for the tip–molecule interactions, the dendritic molecules were tethered to an atomically flat silicon surface through an anchoring, amine-terminated, alkyl-silane self-assembled monolayer (SAM).¹⁹ To avoid high attractive forces, the AFM tips, in turn, were modified with a methyl-terminated SAM.^{19,20}

Experimental Section

Characterization and Micromapping. Experiments were carried on Dimension 3000 and Multimode microscopes. Silicon

*To whom correspondence should be addressed: vladimir@iastate.edu.

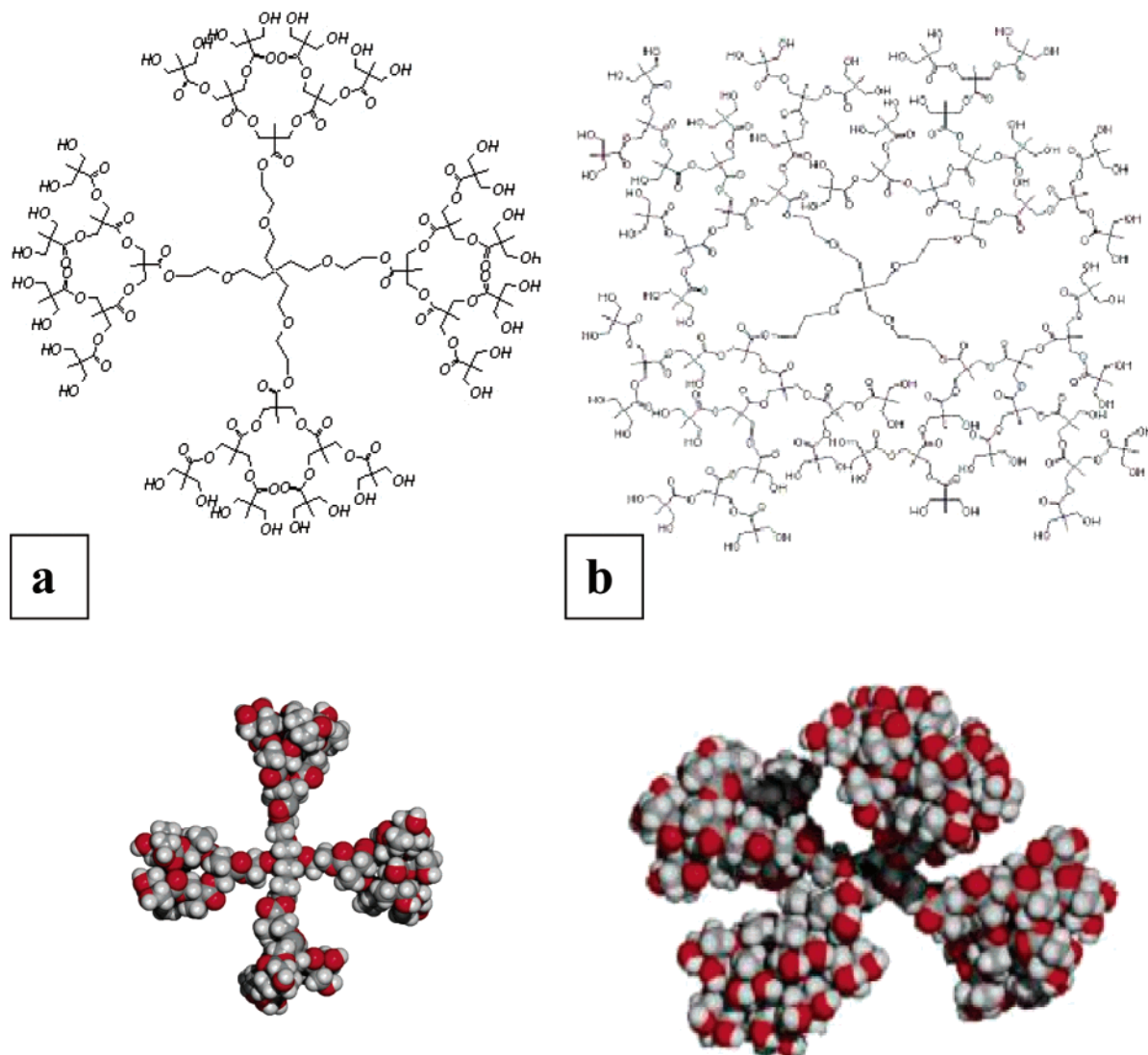


Figure 1. Idealized chemical structure of hyperbranched molecules (top) and corresponding molecular models (bottom) for G3 (a) and G4 (b). The actual chemical microstructure of hyperbranched molecules deviates significantly from the idealized structure presented here with a degree of branching close to 50–60%.

tips CSC12/50 (NT DMT) were selected for this testing. Spring constants were measured and cross-checked by added mass, tip-on-tip, and resonant frequencies methods.²¹ They usually varied from 3.5 to 5.5 N/m. Tip radii varied from 10 to 30 nm as measured on a gold nanoparticle reference standard. Sensitivity of the piezoelement was carefully measured on a bare silicon wafer right before and after probing. Tapping-mode (TM) images were obtained to identify surface areas with appropriate concentration of anchored molecules. FV micromapping with a number of pixels from 16×16 to 64×64 was conducted on several selected locations for selected areas from 200×200 nm to 1000×1000 nm. TM imaging was repeated after micromapping to ensure preservation of initial surface morphology. Independent measurements of Young's modulus for 40 nm thick spin-coated films from hyperbranched polymers were conducted.

FV micromapping was done in a gentle force volume mode with pixel-to-pixel distances of 3–12 nm and local deformation not exceeding 4–6 nm.²² The tip deflection during the compression cycle was measured for each location and converted to the load-indentation curve. Data were analyzed using Hertzian contact mechanics, a double-spring variable constant model, measured tip spring constants, and tip-end shapes to deduce local elastic modulus according to the known procedures and theories.^{10,23,24} The tip approaching velocity varied to ensure that the viscous contribution is insignificant, and

zooming-out scanning was conducted to ensure completely reversible deformation.

Materials. We study third (G3) and fourth (G4) generation dendritic molecules (molecular weights of about 3000–7000, respectively).¹⁴ Commercially available hydroxyl-terminated hyperbranched polyesters were donated by Perstorp Polyol Inc. These molecules possess slightly flattened and spherical conformations on solid substrates with dimensions of about 2.5 and 3 nm for G3 and G4 molecules, respectively (see an idealized chemical architecture in Figure 1).²⁵ Corresponding bulk materials are tough polymers with a relatively high glass transition temperature (82 °C for G4 and 72 °C for G3 as was determined from DSC measurements on a Pyris 1 instrument).

Sample Preparation. The substrates were atomically smooth silicon wafers of the {100} orientation with one side polished (Semiconductor Processing, Co.) and modified silicon wafers with NH_2SAM . Silicon wafers were treated in an ultrasonic bath for 10 min followed by a "piranha" solution (30% concentrated hydrogen peroxide, 70% concentrated sulfuric acid) bath for 1 h. After the "piranha" bath, the samples were rinsed several times with Nanopure water (18 M Ω cm) and dried under a stream of dry nitrogen. Depositions of hyperbranched molecules onto the substrates were carried out by adsorption from acetone solution according to the procedure described earlier.²⁵ Silicon substrates with size of 20×20 mm

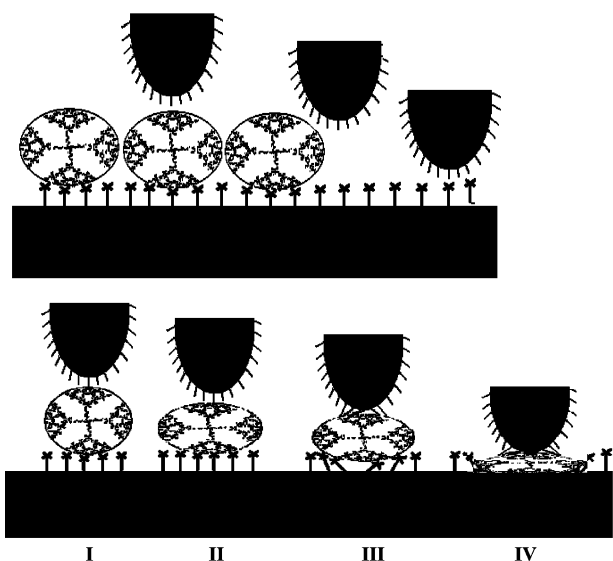


Figure 2. Sketch of dendritic molecules tethered to a silicon surface through anchoring amine-terminated SAM and SAM-modified AFM tip in three different positions during nanomechanical probing: on top of the dendritic molecule, on the border of the of molecular aggregate, and on a SAM-modified silicon surface (top). Bottom: sketch of various stages of deformation of the SAM–dendritic molecule–SAM–AFM tip system. First contact (I), deformation of dendritic molecules (II), further deformation of the dendritic molecules and alkylsilane SAMs on tip and surface (III), and complete compression of all compliant compounds (IV) are shown from left to right.

were put into a 0.5 g/L concentration solution at room temperature for 3 h.

Modification of Silicon Wafers and Tips. Additional functionalized of the tips and substrates is required to facilitate nanomechanical measurements (Figure 2). The modified silicon substrates with NH_2SAM layer were prepared for anchoring hyperbranched molecules. Clean silicon wafers were immersed into about 0.015% NH_2SAM solution in ethanol (100%) (2–3 drops of NH_2SAM in 100 mL of ethanol) for 30 min under conditions of a nitrogen environment and humidity below 5%.^{20,26} After modification, the substrates were rinsed four times with fresh ethanol (95%) under nitrogen and once combining with the ultrasonic bath and then dried with a stream of nitrogen at room temperature.

Silicon tips were modified with methyl-terminated alkylsilane SAM to decrease the adhesion between the AFM tip and hyperbranched molecules. Before modification, the tip was put into a small tube and rinsed two times with a mixed solution of ethanol/chloroform (50/50), and then dried with a stream of nitrogen. The clean tips were immersed in 0.015% (OTS)SAM solution in toluene for 30 min under dry nitrogen condition. The modified tips were rinsed two times with toluene and chloroform and two times with ethanol and then dried with a stream of dry nitrogen. *N*-Octadecyltrichlorosilane (for (OTS)SAM) and (3-aminopropyl)trimethoxysilane (for NH_2SAM) were obtained from Aldrich and Gelest, respectively, purified by distillation, and separately stored into sealed veils. Spectrophotometric grade toluene was purchased from Aldrich and ethyl alcohol (reagent) and acetone (reagent) were purchased from Fisher Scientific Co. and used as received. All the modification processes were performed inside a glovebox filled with dry nitrogen under humidity below 5% and under conditions of a class 100 cleanroom.

Results and Discussion

Figure 3 demonstrates a typical high-resolution topographical image of two different generations of dendritic molecules tethered to the functionalized silicon. The G4 compound formed a random array of individual molecules for a wide range of adsorption conditions as

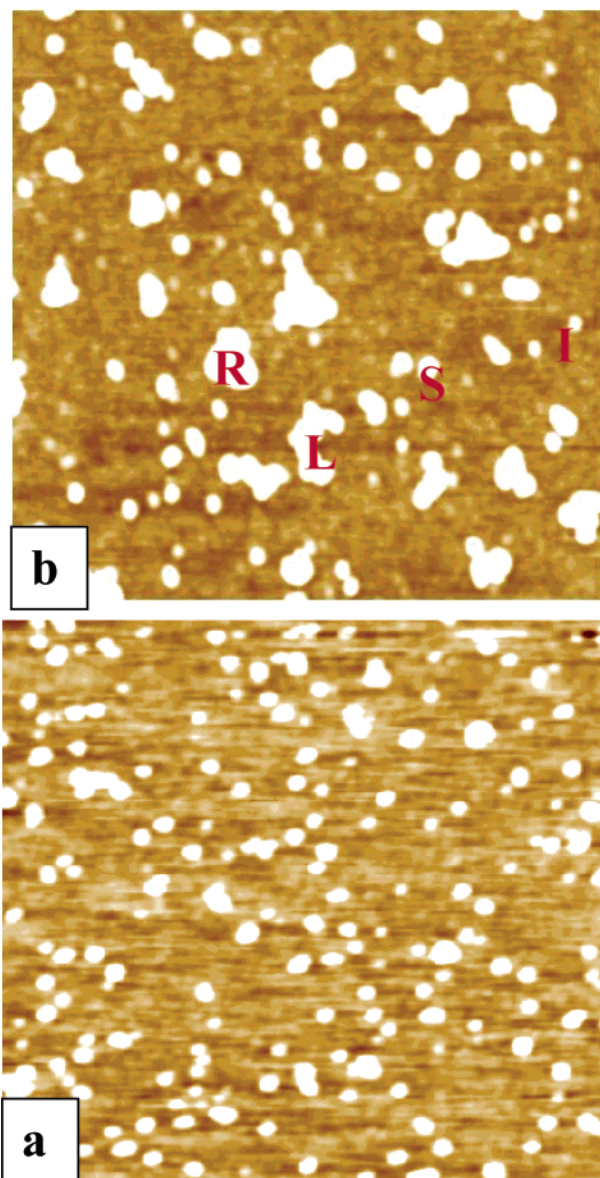


Figure 3. AFM images ($750 \times 750 \times 10$ nm) of anchored dendritic molecules and their aggregates: G4 (a) and G3 (b). Examples of different aggregates for G3 molecules are marked as follows: I, individual molecule; R, round aggregate; S, short-chain aggregate; L, long-chain aggregate.

discussed earlier.²⁵ In contrast, G3 generation dendritic molecules formed a variety of surface aggregates. A number of molecules within aggregates evaluated from molecular dimensions after correction for tip dilation varied from 3 to 40. We observed a coexistence of individual molecules, small round aggregates, along with short-chain and long-chain aggregates as marked in Figure 3. As was demonstrated earlier, G3 molecules form bilayers from compressed molecules within molecular aggregates.²⁵ The G4 compound adsorbed on the solid substrate as predominantly individual molecules with their heights close to a diameter estimated from molecular model (Figures 1 and 3). Such surface morphologies correspond to that observed before for regular dendrimers with different levels of flattened conformations for lower and higher generation dendrimers and under conditions of variable molecule-surface interactions.^{27–30}

Surface distribution of the nanomechanical properties was probed for randomly selected surface areas contain-

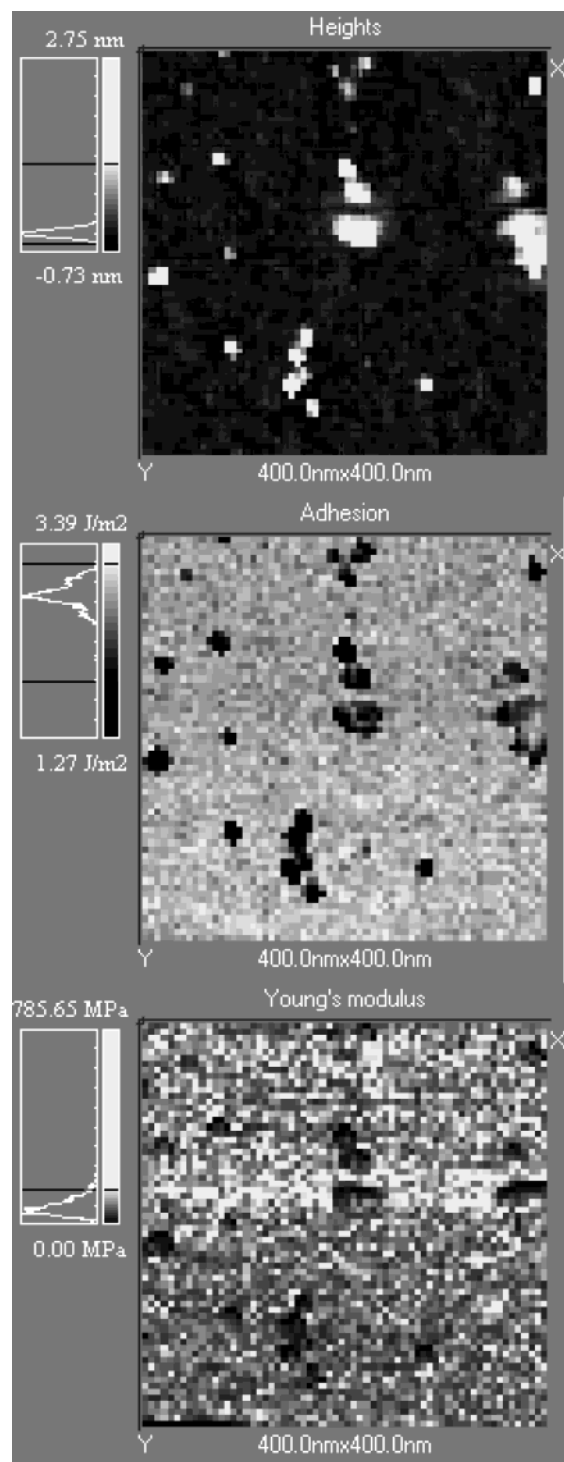


Figure 4. FV analysis of G3 molecular aggregates, 64×64 array, 400×400 nm area: topography (top) and concurrently obtained surface distribution of adhesive forces (middle) and elastic modulus (bottom).

ing at least several clusters of different dimensions (Figures 4 and 5). Despite some random deviations due to a noise contribution and the thermal nanoscale drift within a long time period (more than 1 h for the highest lateral resolution), a clear correlation can be seen between locations and shapes of molecular clusters on the high-resolution AFM TM image and corresponding topographical, adhesion, and elastic modulus images on FV micromaps (Figure 5). As expected, the stiffness of the aggregates of dendritic molecules and individual molecules statistically was much lower than for the

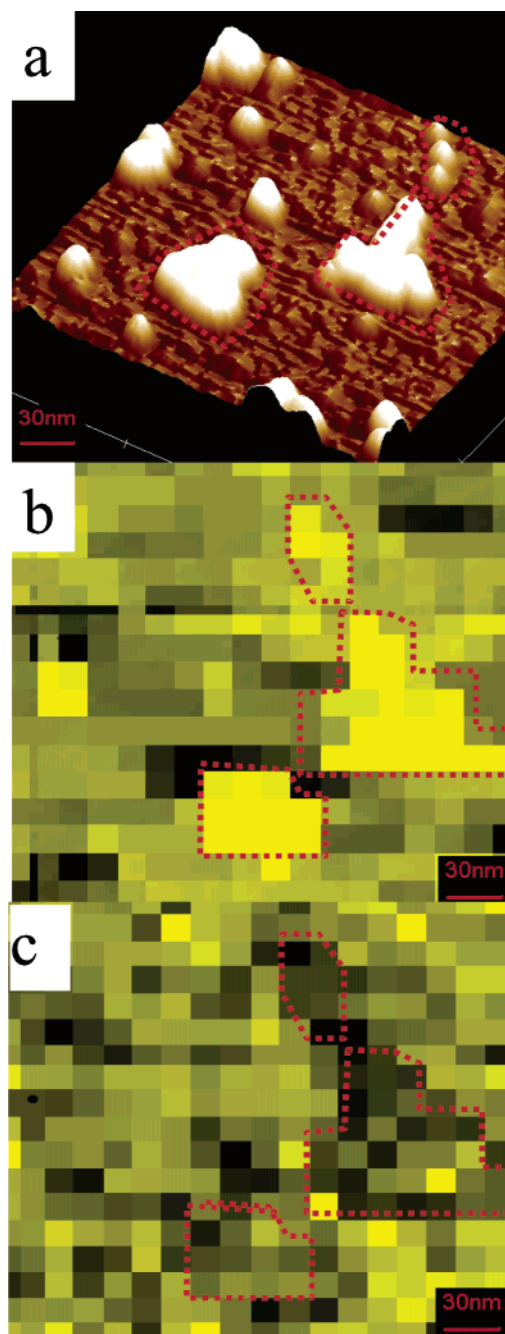


Figure 5. Micromapping of surface aggregates of G3 molecules: (a) 3D TM image of a selected surface area with three different molecular aggregates marked by dotted lines; (b) topographical map (32×32 pixels) of the same surface area with the same molecular aggregates marked by dotted lines; (c) surface distribution of local stiffness with the same molecular aggregates marked by dotted lines.

surrounding SAM-terminated silicon surface. Correspondingly, adhesion is higher for the amine-terminated SAM than for the hydroxyl-terminated dendritic molecules as is expected due to stronger amine–hydroxyl interactions when the AFM tip has partially incomplete modification.²⁰

Force–distance data for the dendritic molecules clearly showed different compression behaviors under low and high normal loads (Figure 6a). An initial jump-in contact did not exceed, usually, 0.5 nm and, thus, did not affect significantly the deformation of the molecules. Immediately after a jump-in contact, a minor tip deflection was observed for first 2–4 nm of piezoelement displace-

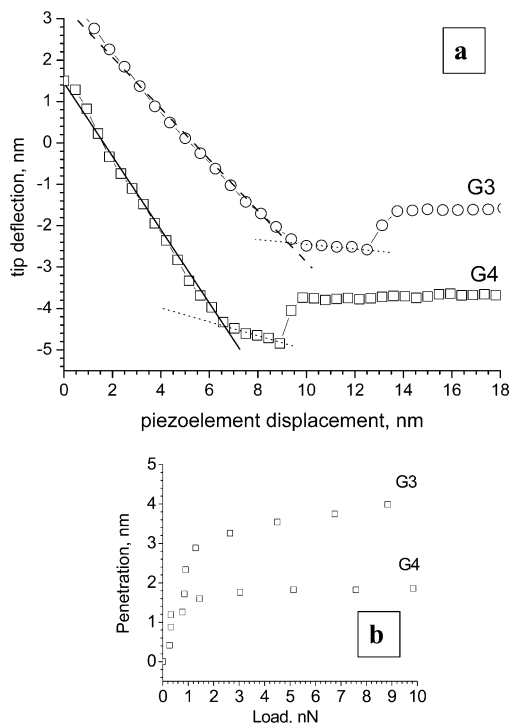


Figure 6. Examples of force–distance curves for individual G3 and G4 molecules with two different ranges of elastic response (a) and corresponding penetration–load curves (b).

ment. This is an indication of a very compliant surface. The FDC slope changed dramatically (several times) under further compression. Correspondingly, indentation–load curves showed two regions of elastic response with different slopes instead of a monotonic variation expected for the elastic deformation of a homogeneous solid (Figure 6b). A large initial deformation of 2–3 nm was detected for low loads below 1 nN. This was followed by much stiffer response with very minor, if any, deformation of the contacting surfaces at higher normal loads. All changes were completely reversible and were consistent for different surface areas and micromapping parameters. The absence of the residual plastic deformation was tested with high-resolution scanning of the surface areas immediately after the probing.

This kind of nanomechanical response is a characteristic of very compliant and thin layer on a stiff solid substrate.^{22,31} Indeed, depth profiles of the elastic modulus presented in Figure 7 for both molecules, possess a characteristic nonmonotonic behavior. For G3 molecules, the elastic modulus of around 200–400 MPa is observed for the initial, 3 nm indentation depth. As can be seen in Figure 7, data points for different molecules are scattered but follow a similar trend. This is followed with a sharp rise, which exceeds the limits of sensitivity (about 3 GPa for this setup) for the indentation depth higher than 5 nm (Figure 7a). The height of G3 molecular layer is about 2.5 nm and the thickness of SAMs on the AFM tip and substrate is about 3 nm. The estimated elastic modulus of SAM layers with alkyl chains is within 1–5 GPa as was shown in several studies.^{32,33} This suggests that they could be compressed under given probing conditions with the average pressure in the contact area reaching 100–200 MPa as estimated from the Hertzian model.

Considering all these circumstances, we suggest the following sequence of elastic deformation processes within the contact area (Figure 2). First, the initial

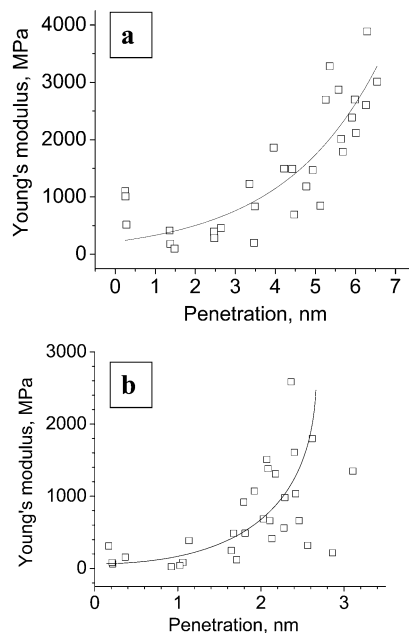


Figure 7. Depth profile of the elastic modulus for G3 (a) and G4 (b). Lines are guides for an eye. Data points are collected for several (three to four) different molecules.

contact involves predominant deformation of the dendritic molecules and an intact state of both substrate and tip SAMs. For very low loads (below 1 nN) and small indentation depth (below 2.5 nm) an elastic compression of the dendritic molecules occurs. Second, for further deformation (next 2–3 nm of the indentation depth), the dendritic molecules became completely “squeezed”. Under higher local pressure, stiffer alkylsilane SAMs on the AFM tip and silicon substrate became subject of elastic deformation themselves. Finally, for even higher normal loads, all organic components became fully compressed and the AFM tip approaches the solid wall, the silicon oxide layer, and further deformation stops. A very similar behavior was observed for stiffer G4 molecules with total elastic deformation reaching 3 nm under similar probing conditions (Figure 7b). Therefore, for further evaluation of the elastic properties of the dendritic molecules, we limited the indentation depth to 2–3 nm by controlling a feedback threshold. We conducted statistical analysis of multiple surface areas to ensure the presence of at least 20–30 individual molecules or aggregates.

Statistical, pixel-by-pixel analysis of the surface distribution of the elastic modulus clearly demonstrated the presence of three distinct levels of the surface stiffness for the dendritic molecules and their aggregates tethered to the silicon surface (Figure 8). These three levels corresponded to tip–dendritic molecules, tip–border dendritic molecules, and tip–substrate interactions mediated by the presence of alkyl chain on the substrate and the AFM tip as depicted in Figure 2.

A first peak, with high elastic modulus of 1.1 GPa, corresponds to the surface areas of the SAM-modified silicon without dendritic molecules. For this type of contacts, the elastic response is determined by deformation of alkyl chains of contacting SAMs of the AFM tips and substrates. The value of the elastic modulus obtained is within the range obtained for the alkyl chain containing monolayers with the AFM tips (1–5 GPa).^{32,33} A broad maximum at lower values of the elastic modulus is composed of two peaks. As was identified by

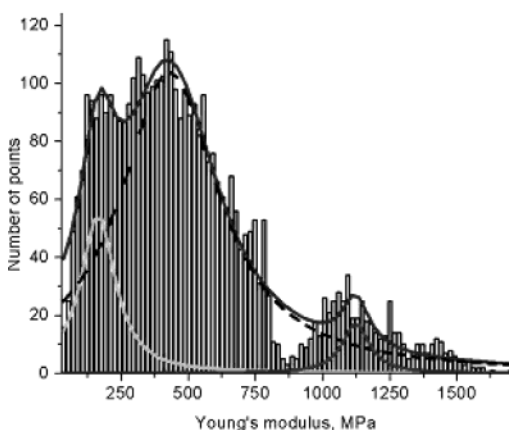


Figure 8. Histogram of the surface distribution of the elastic modulus collected for G3 molecules on the $1 \times 1 \mu\text{m}$ surface area (32×32) showing three different levels of the surface stiffness.

analyzing spatial correlation between different histogram regions and surface areas, these peaks corresponded to the central areas of molecular aggregates and the aggregate borders. The absolute values of the elastic modulus for the dendritic molecules within internal aggregate regions were within the range from 100 to 300 MPa. Border regions showed overestimated elastic modulus values due to the lateral physical contact of the AFM tip and the aggregate edges that increased an actual contact area. On the other hand, the presence of the silicon substrate affects the “apparent” modulus in the case when the AFM tip is engaged with aggregate only on the peripheral region and the very end of the tip is in the contact with the SAM surface (Figure 2). Therefore, for the calculation of the average elastic modulus for the dendritic molecules, we excluded SAM surface contributions and conducted a pixel-by-pixel analysis of different aggregates excluding the aggregate edges.

Within molecular aggregates and for individual molecules, the probing conditions are favorable for interaction of the AFM tip with a single dendritic molecule. Estimation of the radius of the contact area, conducted under the Hertzian approximation, shows that it varies from 1 nm for the lowest load to 3 nm at high load. Thus, the initial tip–molecule contact is localized within a single molecule (molecular diameter is within 2.5–3 nm). Only the largest deformation could result in spreading the contact area beyond a single squeezed molecule and initiated involvement of the neighboring molecules in the deformational process.

We grouped all data collected in four different classes according to the tested object—individual molecules, round aggregates, short-chain aggregates, and long-chain clusters—and calculated separately the average values of the elastic modulus (Figure 3). The elastic modulus of the individual G3 molecules, thus, was determined to be 190 ± 30 MPa (Figure 9). This value is a characteristic of flexible polymers below but close to the glass transition temperature (both dendritic molecules possess glass transition temperatures close to 80°C). Additionally, this value is close to the value measured for corresponding bulk material (160 ± 15 MPa as measured for spin-coated films of G3). This suggests that the individual dendritic molecules possess self-sufficient elastic resistance that does not rely on a network of physical entanglements with surrounding

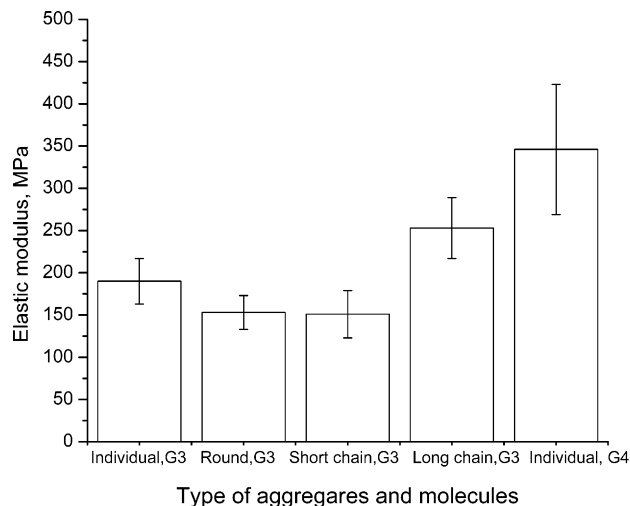


Figure 9. Average elastic modulus obtained for individual dendritic molecules and different types of surface aggregates.

macromolecules such as linear polymers whose elastic response is determined by the length of the segments between physical entanglements.³⁴

The value of the elastic modulus remains similar for small round and short chain aggregates of G3 molecules considering error bars (150 ± 25 MPa) (Figure 9). However, the dendritic molecules aggregated in long-chain clusters (at least 10 molecules long) such as the one marked in Figure 3, possess higher stiffness. The value of the elastic modulus reaches 250 ± 30 MPa, which is comfortably higher than the value of the individual molecules even considering significant error bars due to data scattering for different surface locations (Figure 9). A cause for the increased molecular stiffness of the dendritic molecules aggregated in long-chain clusters remains to be discovered. Here, we could only speculate that the lateral constraints caused by the presence of densely packed neighboring “border” molecules tethered to the supporting substrate play significant role.

Finally, higher generation dendritic molecules G4 revealed a much higher elastic modulus approaching 350 ± 70 MPa (Figure 9). This value reflected the higher internal molecular stiffness of the dendritic molecules with much more crowded shells containing 64 terminal branches.³⁵ In this case, the absence of surface clusters did not allow addressing a role of the surface aggregation on the molecular stiffness of higher generation dendritic molecules.

Acknowledgment. The authors thank S. Peleshanko and D. Julthongpiput for technical assistance, M. LeMieux for useful discussions, and Perstop Polyols for samples donation. Funding from the National Science Foundation, Grants DMR-0074241 and CMS-0099868, is gratefully acknowledged.

References and Notes

- (1) Graighead, H. G. *Science* **2000**, *290*, 1532.
- (2) Bhushan, B.; Israelachvili, J. N.; Landman, U. *Nature (London)* **1995**, *374*, 607.
- (3) Sheiko, S. S. *Adv. Polym. Sci.* **2000**, *151*, 61. Zhang, X.; Klein, J.; Sheiko, S.; Muzafarov, A. M. *Langmuir* **2000**, *16*, 3893. Sheiko, S. S.; Moller, M. *Chem. Rev.* **2001**, *101*, 4099.
- (4) Carrion-Vazquez, M.; Oberhauser, A. F.; Fisher, T. E.; Marszalek, P. E.; Li, H.; Fernandez, J. M. *Prog. Biophys. Mol. Biol.* **2000**, *74*, 63.

- (5) Schneider, M.; Zhu, M.; Papastavrou, G.; Akari, S.; Mohwald, H. *Langmuir* **2002**, *18*, 602.
- (6) Florin, E.-L.; Moy, V. T.; Gaub, H. E. *Science* **1994**, *264*, 415.
- (7) Zhang, W.; Xu, Q.; Zou, S.; Li, H.; Xu, W.; Zhang, X.; Shao, Z.; Kudera, M.; Gaub, H. *Langmuir* **2000**, *16*, 4305.
- (8) Hugel, T.; Grosholz, M.; Clausen-Schaumann, H.; Pfau, A.; Gaub, H.; Seitz, M. *Macromolecules* **2001**, *34*, 1039.
- (9) Yamamoto, S.; Tsujii, Y.; Fukuda, T. *Macromolecules* **2000**, *33*, 5995.
- (10) *Nanoscope III*; Digital Instruments, Santa Barbara, CA, 1995. See review in: Tsukruk, V. V.; Gorbunov, V. V. *Microsc. Today* **2001**, *01-1*, 8 and Tsukruk, V. V.; Gorbunov, V. V. *Probe Microsc.* **2002**, *3-4*, 241.
- (11) Overney, R. M. *Trends Polym. Sci.* **1995**, *3*, 359. Domke, J.; Radmacher, M. *Langmuir* **1998**, *14*, 3320. Vanlandingham, M. R.; McKnight, S. H.; Palmese, G. R.; Eduljee, R. F.; Gillespie, J. W.; McCulough, R. J. *J. Mater. Sci. Lett.* **1997**, *16*, 117. Reynaud, C.; Sommer, F.; Quet, C.; Bounia, N. El.; Duc, T. M. *Surf. Interface Anal.* **2000**, *30*, 185. Du, B.; Tsui, O. K.; Zhang, Q.; He, T. *Langmuir* **1998**, *14*, 2606. Tsukruk, V. V.; Gorbunov, V. V.; Huang, Z.; Chizhik, S. A. *Polym. Int.* **2000**, *49*, 441. Chizhik, S. A.; Huang, Z.; Gorbunov, V. V.; Myshkin, N. K.; Tsukruk, V. V. *Langmuir* **1998**, *14*, 2606.
- (12) Kim, Y. H. *J. Polym. Sci., Polym. Chem.* **1998**, *36*, 1685.
- (13) Voit, B. *J. Polym. Sci., Part A* **2000**, *38*, 2505.
- (14) Mezzenga, R.; Boogh, L.; Manson, J.-A. E.; Pettersson, B. *Macromolecules* **2000**, *33*, 4373.
- (15) Tully, D. C.; Frechet, M. J. *Chem. Commun.* **2001**, *14*, 1229.
- (16) Sheiko, S.; Moller, M. *Top. Curr. Chem.* **2001**, *212*, 137.
- (17) Li, J.; Piehler, L. T.; Qin, D.; Baker, J. R., Jr.; Tomalia, D. A. *Langmuir* **2000**, *16*, 5613.
- (18) Fréchet, J. M. J.; Tomalia, D. A., Eds. *Dendrimers and Other Dendritic Polymers*, John Wiley & Sons: New York, 2002. Frechet, J. M. *Science* **1994**, *263*, 1711. Grayson, S. M.; Frechet, J. M. J. *Chem. Rev.* **2001**, *101*, 3819. Meijer, E. W. *Science* **1994**, *266*, 1226. Frechet, J. M.; Hawker, G. J.; Gitsov, I.; Leon, J. W. *Pure Appl. Chem.* **1996**, *A33*, 1399.
- (19) Ulman, A. *Introduction to Ultrathin Organic Films*, Academic Press: San Diego, CA, 1991. Pluddemann, E. P. *Silane Coupling Agents*, Plenum Press: New York, 1991. Tsubokawa, N.; Kogure, A.; Maruyama, K.; Sone, Y.; Shimomura, M. *Polym. J.* **1990**, *22*, 827. Wasserman, S. R.; Tao Y.-T.; Whitesides, G. M. *Langmuir* **1989**, *5*, 1074. Parikh, A. N.; Liedberg, B.; Atre, S. V.; Ho, M.; Allara, D. L. *J. Phys. Chem.* **1995**, *99*, 9996. Whitesides, G. M.; Laibinis, P. E. *Langmuir* **1990**, *6*, 87. Tsukruk, V. V.; Lander, L. M.; Brittain, W. J. *Langmuir* **1994**, *10*, 996. Tsukruk, V. V.; Luzinov, I.; Julthongpipit, D. *Langmuir* **1999**, *15*, 3029.
- (20) Noy, A.; Vezenov, D. V.; Lieber, C. M. *Annu. Rev. Mater. Sci.* **1997**, *27*, 381. Tsukruk, V. V.; Bliznyuk, V. N. *Langmuir* **1998**, *14*, 446.
- (21) Cleveland, J. P.; Manne, S.; Bocek, D.; Hansma, P. K. *Rev. Sci. Instrum.* **1993**, *64*, 403. Hazel, J. L.; Tsukruk, V. V. *Thin Solid Films* **1999**, *339*, 249.
- (22) Tsukruk, V. V.; Sidorenko, A.; Gorbunov, V. V.; Chizhik, S. A. *Langmuir* **2001**, *17*, 6715.
- (23) Phart, G. M.; Oliver, W. C.; Brotzen, F. B. *J. Mater. Res.* **1992**, *7*, 613. Johnson, K. L.; Kendall, K.; Roberts, A. D. *Proc. R. Soc., London* **1971**, *A324*, 301. Tsukruk, V. V.; Huang, Z.; Chizhik, S. A.; Gorbunov, V. V. *J. Mater. Sci.* **1998**, *33*, 4905. Tsukruk, V. V. *Rubber Chem. Technol.* **1997**, *70(3)*, 430.
- (24) Tsukruk, V. V.; Huang, Z. *Polymer* **2000**, *41*, 5541.
- (25) Sidorenko, A.; Zhai, X. W.; Peleshanko, S.; Greco, A.; Shevchenko, V. V.; Tsukruk, V. V. *Langmuir* **2001**, *17*, 5924.
- (26) Tsukruk, V. V.; Nguyen, T.; Lemieux, M.; Hazel, J.; Weber, W. H.; Shevchenko, V. V.; Klimenko, N.; Sheludko, E. In *Tribology Issues and Opportunities in MEMS*; Bhushan, B.; Kluwer Academic Publ.: Dordrecht, The Netherlands, 1998; p 608.
- (27) Betley, T.; Holl, M.; Orr, B.; Swanson, D.; Tomalia, D.; Baker, Jr, J. *Langmuir* **2001**, *17*, 2768. Betley, T.; Hessler, J. A.; Mecke, A.; Holl, M.; Orr, B.; Uppuluri, S.; Tomalia, D.; Baker, Jr, J. *Langmuir* **2002**, *18*, 3127.
- (28) Tokuhisa, H.; Zhao, M.; Baker, L.; Phan, V.; Dermody, D.; Garcia, M.; Peez, R.; Crooks, R.; Mayer, T. *J. Am. Chem. Soc.* **1998**, *120*, 4492. Hierlemann, A.; Campbell, J. K.; Baker, L. A.; Crooks, R. M.; Ricco, A. J. *J. Am. Chem. Soc.* **1998**, *120*, 5323.
- (29) Mansfield, M. L. *Polymer* **1996**, *37*, 3835.
- (30) Tsukruk, V. V. *Adv. Mater.* **1998**, *10*, 253. Tsukruk, V. V.; Rinderspacher, F.; Bliznyuk, V. N. *Langmuir* **1997**, *13*, 2171. Bliznyuk, V. N.; Rinderspacher, F.; Tsukruk, V. V. *Polymer* **1998**, *39*, 5249.
- (31) Tsukruk, V. V.; Sidorenko, A.; Yang, H. *Polymer* **2002**, *43*, 1695. Tsukruk, V. V.; Ahn, H.-S.; Sidorenko, A.; Kim, D. *Appl. Phys. Lett.* **2002**, *80*, 4825.
- (32) Tsukruk, V. V.; Bliznyuk, V. N.; Hazel, J.; Visser, D.; Everson, M. P. *Langmuir* **1996**, *12*, 4840. Bliznyuk, V. N.; Everson, M. P.; Tsukruk, V. V. *J. Tribol.* **1998**, *120*, 489.
- (33) Xiao, X.; Hu, J.; Charych, D. H.; Salmeron, M. *Langmuir* **1996**, *12*, 235. Oishi, Y.; Umeda, T.; Kuramori, M.; Suehiro, K. *Langmuir* **2002**, *18*, 945.
- (34) Sperling, L. *Introduction in Physical Polymer Science*, 3rd ed.; Wiley-Interscience: New York, 2001.
- (35) Newkome, G. R.; Moorefield, C. N.; Vogtle, F., Eds. *Dendritic Molecules*; VCH: Weinheim, Germany, 1996.